Enabling quantum sensing under extreme pressure: Nitrogen-vacancy magnetometry up to 130 GPa

Antoine Hilberer, Loïc Toraille, Cassandra Dailledouze, Marie-Pierre Adam, Liam Hanlon, Gunnar Weck, Martin Schmidt, Paul Loubeyre, Jean-François Roch

Letter

Enabling quantum sensing under extreme pressure: Nitrogen-vacancy magnetometry up to 130 GPa

Antoine Hilberer,[1,2,3] Loïc Toraille,[2,3] Cassandra Dailledouze,[1] Marie-Pierre Adam,[1] Liam Hanlon,[1] Gunnar Weck,[2,3] Martin Schmidt,[1] Paul Loubeyre,[2,3] and Jean-François Roch[1,*]

[1]*Université Paris-Saclay, CNRS, ENS Paris-Saclay, CentraleSupelec, LuMIn, F-91190 Gif-sur-Yvette, France*

[2]*CEA DAM DIF, F-91297 Arpajon, France*

[3]*Université Paris-Saclay, CEA, Laboratoire Matière en Conditions Extrêmes, F-91680 Bruyères-le-Châtel, France*

(Received 12 January 2023; revised 8 March 2023; accepted 2 June 2023; published 13 June 2023)

Engineering a layer of nitrogen-vacancy (NV) centers on the tip of a diamond anvil creates a multipurpose quantum sensor array for high-pressure measurements, especially for probing the magnetic and superconducting properties of materials. Expanding this concept above 100 GPa appears to be a substantial challenge. We observe that deviatoric stress on the anvil tip sets a limit at 40–50 GPa for practical magnetic measurements based on the optically detected magnetic resonance (ODMR) of NV centers under pressure. We show that this limit can be circumvented up to at least 130 GPa by machining a micropillar on the anvil tip to create a quasihydrostatic stress environment for the NV centers. Improved hydrostaticity is quantified using the pressure dependence of the diamond Raman shift, the NV ODMR dependence on applied magnetic field, and NV photoluminescence spectral shift. This paves the way for the reliable use of NV microsensing at pressures above 100 GPa.

DOI: 10.1103/PhysRevB.107.L220102

Introduction. The application of pressures above 100 GPa leads to the stability of new phases of matter with remarkable properties such as metallic hydrogen [1], superconductivity close to ambient temperature in superhydrides [2–4], and superionic water ice [5]. Such pressures can only be achieved in static conditions using a diamond anvil cell (DAC) [6]. While structural measurements of samples in the DAC are routinely performed using x-ray spectroscopy, the *in situ* characterization of magnetic or superconducting properties has proven difficult. Measurements of magnetic susceptibilities are mainly done using flux detection by inductive coils [7] or by integrating a miniaturized DAC in a superconducting interference device (SQUID) [8]. Since the DAC limits the sample size to a few micrometers at pressures above 100 GPa, the signal must be extracted from a large background originating from the DAC apparatus, leading to a decrease of the sensitivity with pressure.

Recent works demonstrated a possible alternative by integrating diamond nitrogen-vacancy (NV) centers into the DAC in order to detect the stray magnetic field created by the sample [9–12]. By putting the NV centers directly in contact with the sample, the magnetic detection has micrometer spatial resolution and its sensitivity is independent of the sample size down to the micrometer scale. This NV microsensing method can be easily combined with synchrotron x-ray characterizations to correlate the magnetic or superconducting properties with a well-defined crystallographic structure [13]. However, the existence of a possible pressure limit to NV microsensing remains an open question.

Here, we investigate the pressure dependence of NV magnetic microsensing. We show that the existence of deviatoric stress in the diamond anvil sets an effective limit of about 50 GPa to the magnetic response of NV centers localized at the anvil tip [9,10]. By milling a micropillar in the anvil tip we ensure a quasihydrostatic stress environment that allows us to extend NV magnetometry to 130 GPa. This paves the way for the reliable application of NV microsensing for measurements of magnetic phenomena at extreme pressures.

Experimental configuration. The negatively charged NV center is a point defect of diamond that emits visible photoluminescence (PL) by absorbing green photons and reemitting red photons (at ambient pressure), with an electronic spin $s = 1$ in the ground and excited states. In the absence of external magnetic and stress fields, the $m_s = \pm 1$ spin sublevels of the ground state are degenerate and separated by $D = 2.87$ GHz from the $m_s = 0$ sublevel [Fig. 1(a)]. Spin-dependent PL arises from a spin-selective difference in the nonradiative coupling to metastable singlet states, which also induces optical pumping into the $m_s = 0$ state under green illumination [14]. The energy difference between the sublevels of the ground state can then be read out from the change of the NV luminescence intensity upon scanning the frequency of an additional microwave excitation. Dips in the PL intensity indicate that the excitation microwave frequency is resonant with a transition between two sublevels, leading to optically detected magnetic resonance (ODMR) that can be easily implemented by addressing the NV centers through the diamond anvil [9].

We use the same experimental configuration as in Ref. [9], keeping two crucial characteristics: (1) The NV centers are integrated into the DAC device by mounting a IIas ultrapure Almax-Boehler design [100]-cut diamond anvil with a dense ensemble of NV centers (typically 10^4 NV/μm^2) implanted at about 20 nm beneath the anvil surface using a nitrogen focused ion beam (FIB) [15] [Fig. 1(b)]; (2) the microwave

*jean-francois.roch@ens-paris-saclay.fr

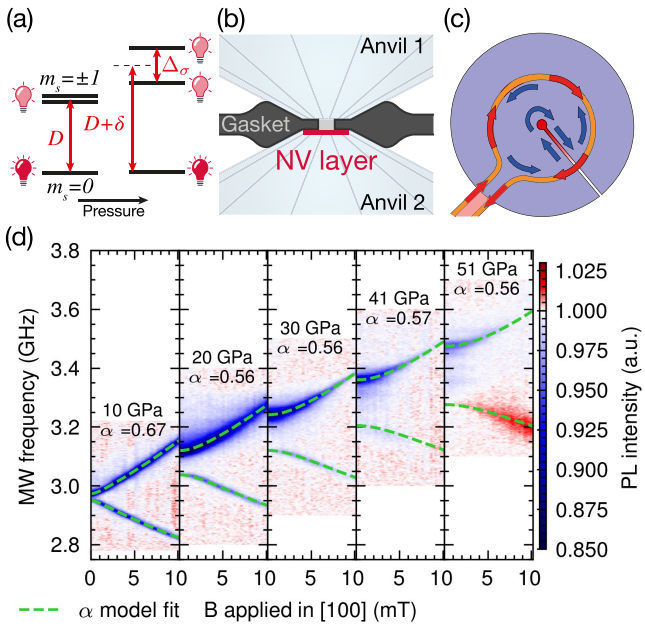

FIG. 1. (a) Energy diagram of the NV center ground state and evolution under stress. (b) Schematic cross section of the location of NV centers implanted as a layer below the anvil culet surface. (c) Design of the machined gasket compatible with the MW excitation of the NV centers. Red arrows show the initial MW excitation current in the wire loop, and blue arrows are currents induced into the gasket. The areas shaded in red indicate the intensity of the MW field. (d) ODMR spectra of NV centers implanted in the tip of a standard diamond anvil at different pressures, as a function of a magnetic field applied along the [100] diamond axis. Green dashed lines are fits of the eigenfrequencies computed with the NV ground state Hamiltonian given by Eq. (1).

excitation is applied using an external single-turn coil above the rhenium gasket of the DAC. The metallic gasket is machined with a slit, filled with an epoxy-glue mixture ensuring sample confinement and DAC mechanical stability. This slit redistributes the induced currents in the metal, leading to focusing and amplification of the microwave flux in the sample chamber similarly to a Lenz lens [16] [Fig. 1(c)]. Upon pressure increase, the PL excitation wavelength was decreased to match the blueshift of the NV absorption spectrum [17] by using continuous-wave (cw) lasers at successive wavelengths 532, 488, 457, and 405 nm. A customized confocal optical microscope was used to collect the PL. A static vector magnetic field was applied on the DAC using three Helmholtz coil pairs with an amplitude ranging between 0 and 10 mT. The magnetic field was aligned along the DAC axis with accuracy $\pm 0.5^\circ$. This orientation corresponds to the diamond [100] crystal axis for which all NV centers have an equivalent responses to stress and magnetic field. Pressure in the DAC was measured using the calibrated diamond Raman phonon mode at the anvil tip [18,19].

Stress effect on the dependence to magnetic field. We performed cw-ODMR experiments on the NV centers under pressures ranging from 10 to 70 GPa. At each pressure point, we collected the ODMR spectrum for the ensemble of NV centers under varying amplitude of the applied magnetic field.

The data are shown in Fig. 1(d). In the absence of a magnetic field, the stress applied to the NV centers has three main effects on the ODMR signals. First, the zero-field center frequency $D = 2.87$ GHz increases almost linearly with a slope of 9.6 MHz/GPa to a value $D + \delta$, where δ is the pressure-induced variation [17]. Second, a splitting Δ_σ appears between the transition lines. This splitting increases almost linearly with pressure with a slope of 3.9 MHz/GPa and originates in deviatoric stress at the anvil culet [9,10]. Third and most importantly for practical measurements, the overall observed ODMR contrast decreases severely under pressure [17].

The data also show that, at a given pressure, the quasilinear evolution of the Zeeman splitting due to the applied magnetic field is recovered only above a compensating amplitude of the magnetic field that increases with pressure. This detrimental influence of stress combined with decreased ODMR contrast weakens the NV sensing magnetic sensitivity [9]. Note that the bias magnetic field is not aligned with a given NV axis so as to overlap responses from all NV orientations. This partially off-axis magnetic field mixes the sublevels of the ground state. This mixing perturbs the optically induced spin polarization and quenches the PL [20]. We also observe that in the regime of strong anisotropic stress the contrast of the low-frequency branch becomes gradually smaller than the high-frequency branch. This effect is due to the excitation with a linearly polarized MW magnetic field on the mixed states between $m_s = \pm 1$ induced by the anisotropic stress (see Supplemental Material [21]). After vanishing at a pressure around 40 GPa, a slightly positive contrast reappears (an increase of PL at resonance) above 50 GPa under high enough magnetic field. This inversion of contrast could be due to state mixing in the excited state manifold created by the anisotropic stress, leading to a reordering of state-dependent PL.

In the diamond lattice under mechanical stress (or equivalently strain), the Hamiltonian describing the NV center ground state is modified by a spin-mechanical interaction [22,23] related to the stress tensor $\overleftrightarrow{\sigma}$. The stress tensor must exhibit the cylindrical symmetry of the anvil. At the anvil tip corresponding to a (100) crystallographic plane, the stress components parallel ($\sigma_\parallel$) and perpendicular ($\sigma_\perp$) to the surface differ. Due to continuity of the normal stress component, $\sigma_\perp$ is equal to the experimental pressure P in the DAC chamber. The tangential component $\sigma_\parallel$ is reduced by a factor α compared to $\sigma_\perp$. Using a simplified model of a semi-infinite anvil with a flat face and a circularly symmetric distribution of pressure applied to this face, the α parameter was estimated about 0.6 [24]. Neglecting off-diagonal shear stress components, the stress tensor then reads as

$$\overleftrightarrow{\sigma} = \begin{pmatrix} \alpha P & 0 & 0 \\ 0 & \alpha P & 0 \\ 0 & 0 & P \end{pmatrix}. \tag{1}$$

Using this stress tensor, the diagonalization of the NV ground state Hamiltonian yields modified spin resonance frequencies which can be approximated to first order as

$$\nu_\pm = D + \delta \pm \Delta/2, \tag{2}$$

where δ is the spectral shift due to compression, and $\Delta = \sqrt{\Delta_\sigma^2 + \Delta_B^2}$ is the quadratic sum of the splittings respectively induced by the stress and by the magnetic field (see Supplemental Material [21] for the full expression). Since Eq. (2) is exact only for low off-axis magnetic field, a numerical diagonalization was used to accurately fit the measured resonance frequencies, as shown by the green dashed lines in Fig. 1(d). Only two parameters, α and P, are hence needed to predict the magnetic field response under stress. We obtained a value $\alpha = 0.56$ that is essentially constant with pressure, quantifying deviatoric stress close to the 0.6 value given in Ref. [24].

Deviatoric stress thus introduces major modifications to the NV behavior as the anisotropic compression of the diamond host lattice distorts the C_{3v} symmetry of the NV center. Here, we quantified changes within the NV ground triplet states, but the stress dependence of the singlet states and the excited triplet states remains unexplored and is difficult to assess. As a hypothesis, we attribute the observed modification and ultimate loss of ODMR contrast to the effect of deviatoric stress on these levels involved in the contrast mechanism [25]. This hypothesis is corroborated by recent results obtained on microdiamonds compressed quasihydrostatically inside the sample chamber of a DAC, for which the ODMR signal could be conserved up to 140 GPa [26]. These results converge toward a possible circumventing strategy by ensuring hydrostatic compression of the NV centers.

Restoring hydrostaticity with diamond microstructuration. A strategy to try to mitigate deviatoric stress can be implemented by microstructuring the diamond anvil culet. A successful geometry is presented in Fig. 2(a). A pillar, 7 μm in diameter with a 2-μm-deep trench around it, was FIB-machined on an NV-implanted diamond anvil culet. The pillar surface is thus disconnected from the anvil surface submitted to deviatoric stress induced by anvil cupping tension [27,28]. This also allows the pressure-transmitting medium (PTM) to fill the trench to immerse the pillar in a stress field close to hydrostatic conditions. The pillar is then equivalent to a diamond microdisk that would be integrated into the sample chamber of the DAC but ensures perfect reproducibility and removes any interface with the diamond culet to optimize PL measurements. As seen below, this design is also very robust and can withstand extreme pressures.

The hydrostaticity of the stress exerted on diamond under pressure can be tested by measuring the Raman frequency of the diamond optical phonon. Under hydrostatic conditions, the dependence of the frequency of the Raman scattering with diamond volume follows a Grüneisen relation of parameter $\gamma = 0.97(1)$ whereas the frequency shift is smaller under deviatoric stress [19]. As seen in Fig. 2(c), the Raman spectra measured at the diamond anvil culet on the micropillar and away from it differ. In both cases, the broad asymmetric peak is associated with the stress distribution within the thickness of the anvil that is optically probed, and the high-frequency edge is used to estimate the pressure [18]. At the micropillar, a well-separated peak appears with a higher-frequency shift. The pressure evolution of its center wave number perfectly matches the value obtained for diamond under hydrostatic pressure [19] as shown in Fig. 2(d). This indicates that the tip of the micropillar hosting part of the NV center layer is then close to hydrostatic pressure.

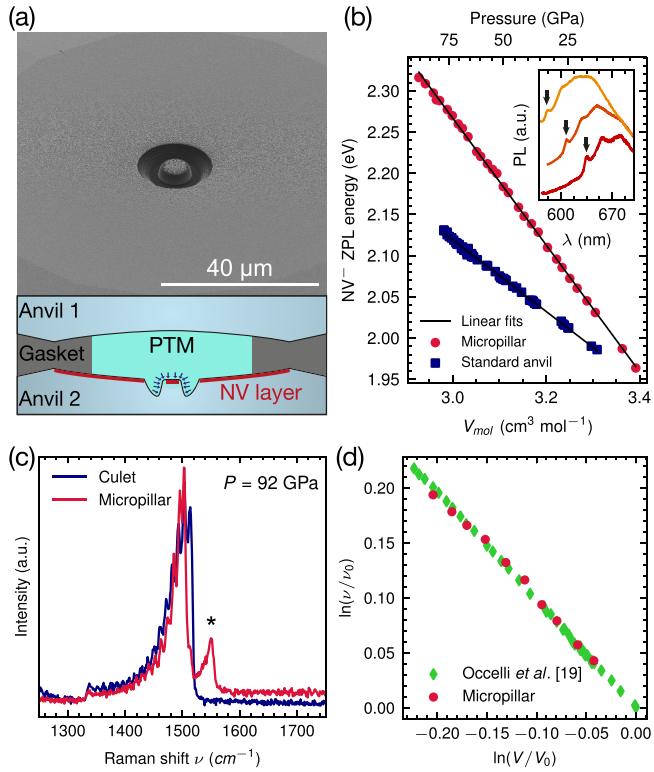

FIG. 2. (a) Scanning electron microscope image of a FIB-machined micropillar on a diamond anvil culet of 100 μm diameter. The bottom panel shows a schematic cross section of the distortion of the culets under pressure. The sample volume of the DAC is only filled with the pressure transmitting medium (PTM). (b) Energy of the NV center zero-phonon line (ZPL) as a function of pressure and diamond volume, recorded for NV centers implanted in and out of the micropillar. Inset: Typical PL spectra of the NV centers recorded at 0, 37, and 78 GPa (bottom to top). The arrows indicate the ZPL position. (c) Diamond Raman spectra recorded on a pressurized microstructured diamond anvil at 92 GPa, on and outside the micropillar. In the spectrum taken on the micropillar, the peak indicated by the star reveals hydrostatic compression. (d) Raman frequency shift measured on the micropillar as a function of relative diamond volume. Data from Ref. [19] references the Raman shift of diamond under hydrostatic pressure.

Accordingly, the PL spectrum of the NV layer in the micropillar shows a pressure-induced blueshift [Fig. 2(b)] that can be quantified with the zero-phonon line (ZPL) [17]. While the NV ZPL dependence with pressure is not linear, its evolution becomes linear when plotted versus the compressed diamond volume estimated using the diamond equation of state [29]. A linear fit gives a slope of -769 ± 4 meV/(cm^3 mol^{-1}). A similar measurement performed on a nonmodified diamond anvil yields a weaker slope of -434 ± 2 meV/(cm^3 mol^{-1}). This significant difference in the pressure dependence of the ZPL is another indication of the deviatoric stress reduction caused by the microstructuration of the anvil tip.

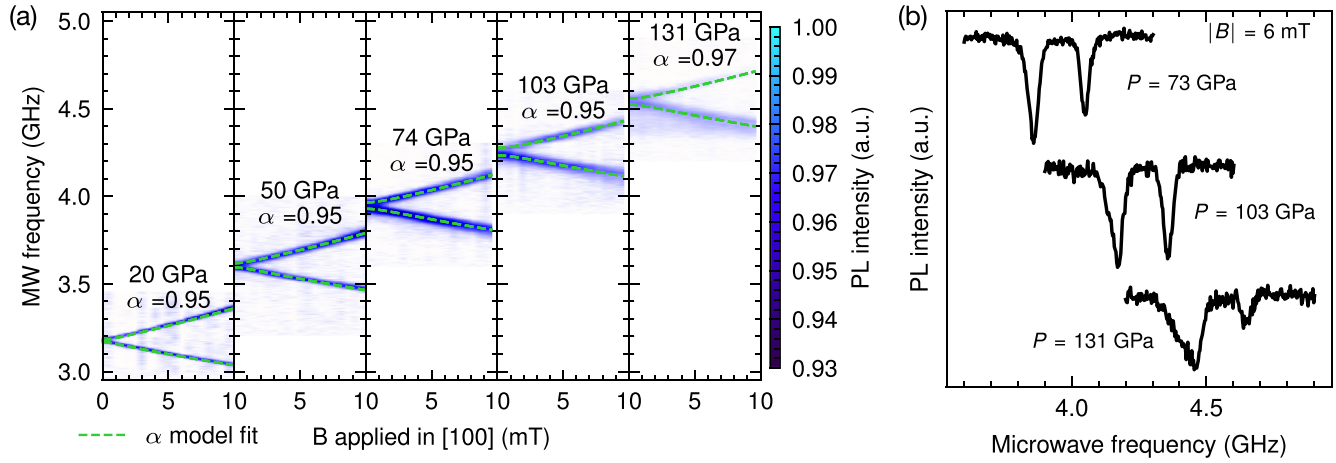

FIG. 3. (a) ODMR spectra obtained from NV centers implanted in a micropillar at varying pressures, as a function of magnetic field applied along the diamond [100] axis. Fitted values of the stress anisotropy parameter $\alpha \simeq 0.95$ indicate quasihydrostatic conditions. (b) ODMR spectra recorded for NV centers in the micropillar for a magnetic field of 6 mT amplitude. The signals at 73, 103, and 131 GPa are normalized for clarity, with contrast values of 5%, 3%, and 1.5%, respectively.

ODMR measurements were also performed for the NV centers hosted in the micropillar. As shown in Fig. 3 corresponding to the pressure evolution up to 130 GPa, most of the detrimental effects previously observed and attributed to deviatoric stress are now suppressed. The spectra consistently show a negative contrast remaining almost constant up to at least 100 GPa. Increasing further the pressure up to 130 GPa (where the experiment was stopped by one of the anvils breaking), a slight decrease of the contrast was observed and is attributed to a degraded efficiency of the microwave excitation for frequencies higher than 4 GHz. Observed ODMR lines exhibit a width that slightly increases with applied pressure, most likely because of a stress inhomogeneity within the probed diamond volume of the micropillar. Broadening due to NV orientation differences induced by deformation of the pillar is ruled out by the observed constant linewidth with increased applied magnetic field at a given pressure. The magnetic field response also remains unchanged across the whole tested pressure range. The ODMR spectra exhibit a very low zero-field splitting Δ_σ of 0.29 ± 0.03 MHz/GPa with increasing pressure, and a shift of the zero-field center frequency $D + \delta$ of 13.42 ± 0.14 MHz/GPa. As shown in Fig. 4 these values differ significantly from those measured for NV centers in standard anvils and were consistent across four experimental runs performed on different anvils, with pillars machined either using a FIB or a femtosecond laser. Applying the model described above for the spin-mechanical interaction, the evolution of the ODMR eigenfrequencies versus the applied magnetic field was well fitted using an anisotropy parameter $\alpha \simeq 0.95$ that stays constant within the pressure range tested [Fig. 3(a)]. Since $\alpha \simeq 1$ would indicate perfect hydrostaticity, this result gives an independent confirmation of the almost hydrostatic pressure applied on the NV centers in the micropillar. Consequently, the microstructuration strategy enables efficient magnetic field sensing at pressures higher than 100 GPa with a sensitivity improved by orders of

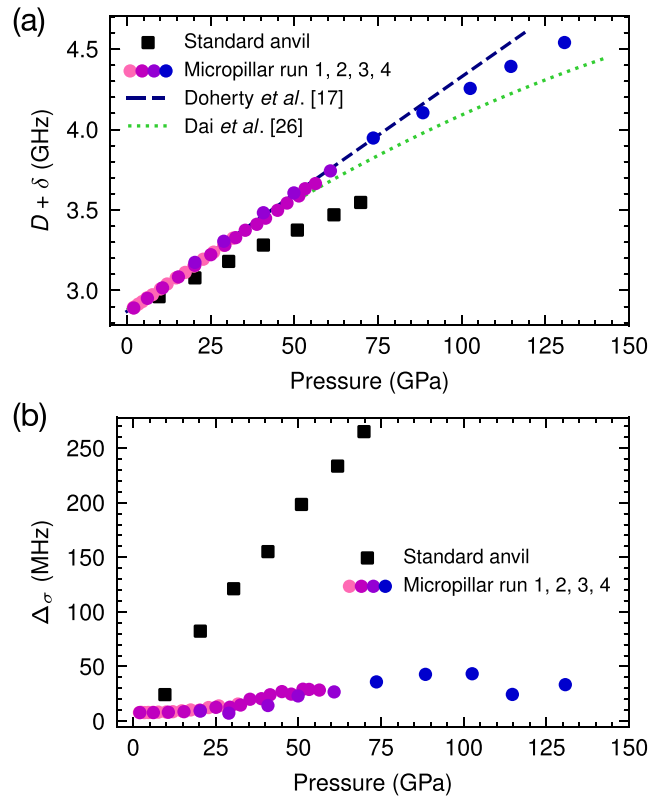

FIG. 4. (a) Pressure dependence of ODMR center frequency $D + \delta$, showing a quasilinear shift of 13.42 ± 0.14 MHz/GPa on the micropillar compared to 9.68 ± 0.8 MHz/GPa on the standard anvil. The extrapolation of the values measured up to 60 GPa in Ref. [17] and the fit up to 140 GPa from Ref. [26] are given for comparison. (b) Pressure dependence of ODMR frequency splitting Δ_σ at zero magnetic field. At the micropillar, Δ_σ increases by 0.29 ± 0.03 MHz/GPa instead of 3.89 ± 0.06 MHz/GPa with the standard geometry of the anvil.

magnitude compared to the use of a standard anvil with a flat tip (see Supplemental Material [21]).

Conclusion. Microstructuration of diamond anvils, implemented here by machining a micropillar on the culet, provides quasihydrostatic conditions for NV centers implanted in the anvil up to 100 GPa and above. With this design NV magnetic sensing can be implemented under such extreme pressures as if at ambient pressure. This work opens the way to sensitive and spatially resolved magnetic measurements in the constrained environment of the DAC, which have been lacking so far. For instance, this method could be used for a convincing observation of the Meissner effect in superhydrides. It should also enable the high-pressure community to exploit the vast diversity of NV-based quantum sensing protocols that have for now been mostly restricted to room pressure, for improving the sensitivity of magnetic detection [30], for detecting current fluctuations using noise spectroscopy [31], and for implementing NMR spectroscopy [32].

Note added. Recently, we became aware of related work by Ho *et al.* [33]. They independently developed a similar model of the stress applied within a DAC to compare results obtained on NV-doped nanodiamonds and implanted NV centers, up to 8 GPa. They also reached the conclusion that hydrostaticity of applied stress could be improved by implementing a pillar structure, which they simulated with finite element methods.

Acknowledgments. We are grateful to Olivier Marie and Grégoire Le Caruyer for machining of the diamond culets, to Florent Occelli for assistance in DAC preparation, and to Dorothée Colson and Anne Forget for annealing the diamond anvils after nitrogen implantation. This work has received funding from the EMPIR program cofinanced by the Participating States and the European Union's Horizon 2020 research and innovation program (20IND05 QADeT), from the Agence Nationale de la Recherche under the project SADAHPT and the ESR/EquipEx + program (Grant No. ANR-21-ESRE-0031), and from the Paris Île-de-France Région in the framework of DIM SIRTEQ. J.F.R. acknowledges support from Institut Universitaire de France.

[1] P. Loubeyre, F. Occelli, and P. Dumas, Nature (London) **577**, 631 (2020).
[2] J. A. Flores-Livas, L. Boeri, A. Sanna, G. Profeta, R. Arita, and M. Eremets, Phys. Rep. **856**, 1 (2020).
[3] A. P. Drozdov, P. P. Kong, V. S. Minkov, S. P. Besedin, M. A. Kuzovnikov, S. Mozaffari, L. Balicas, F. F. Balakirev, D. E. Graf, V. B. Prakapenka, E. Greenberg, D. A. Knyazev, M. Tkacz, and M. I. Eremets, Nature (London) **569**, 528 (2019).
[4] M. Somayazulu, M. Ahart, A. K. Mishra, Z. M. Geballe, M. Baldini, Y. Meng, V. V. Struzhkin, and R. J. Hemley, Phys. Rev. Lett. **122**, 027001 (2019).
[5] G. Weck, J.-A. Queyroux, S. Ninet, F. Datchi, M. Mezouar, and P. Loubeyre, Phys. Rev. Lett. **128**, 165701 (2022).
[6] H.-K. Mao, X.-J. Chen, Y. Ding, B. Li, and L. Wang, Rev. Mod. Phys. **90**, 015007 (2018).
[7] X.-J. Chen, V. V. Struzhkin, Y. Yu, A. F. Goncharov, C.-T. Lin, H.-k. Mao, and R. J. Hemley, Nature (London) **466**, 950 (2010).
[8] V. S. Minkov, S. L. Bud'ko, F. F. Balakirev, V. B. Prakapenka, S. Chariton, R. J. Husband, H. P. Liermann, and M. I. Eremets, Nat. Commun. **13**, 3194 (2022).
[9] M. Lesik, T. Plisson, L. Toraille, J. Renaud, F. Occelli, M. Schmidt, O. Salord, A. Delobbe, T. Debuisschert, L. Rondin, P. Loubeyre, and J.-F. Roch, Science **366**, 1359 (2019).
[10] S. Hsieh, P. Bhattacharyya, C. Zu, T. Mittiga, T. J. Smart, F. Machado, B. Kobrin, T. O. Höhn, N. Z. Rui, M. Kamrani, S. Chatterjee, S. Choi, M. Zaletel, V. V. Struzhkin, J. E. Moore, V. I. Levitas, R. Jeanloz, and N. Y. Yao, Science **366**, 1349 (2019).
[11] K. Y. Yip, K. O. Ho, K. Y. Yu, Y. Chen, W. Zhang, S. Kasahara, Y. Mizukami, T. Shibauchi, Y. Matsuda, S. K. Goh, and S. Yang, Science **366**, 1355 (2019).
[12] Y.-X. Shang, F. Hong, J.-H. Dai, H. Yu, Y.-N. Lu, E.-K. Liu, X.-H. Yu, G.-Q. Liu, and X.-Y. Pan, Chin. Phys. Lett. **36**, 086201 (2019).
[13] L. Toraille, A. Hilberer, T. Plisson, M. Lesik, M. Chipaux, B. Vindolet, C. Pépin, F. Occelli, M. Schmidt, T. Debuisschert, N. Guignot, J.-P. Itie, P. Loubeyre, and J.-F. Roch, New J. Phys. **22**, 103063 (2020).
[14] M. W. Doherty, N. B. Manson, P. Delaney, F. Jelezko, J. Wrachtrup, and L. C. Hollenberg, Phys. Rep. **528**, 1 (2013).
[15] M. Lesik, P. Spinicelli, S. Pezzagna, P. Happel, V. Jacques, O. Salord, B. Rasser, A. Delobbe, P. Sudraud, A. Tallaire, J. Meijer, and J.-F. Roch, Phys. Status Solidi A **210**, 2055 (2013).
[16] T. Meier, N. Wang, D. Mager, J. G. Korvink, S. Petitgirard, and L. Dubrovinsky, Sci. Adv. **3**, eaao5242 (2017).
[17] M. W. Doherty, V. V. Struzhkin, D. A. Simpson, L. P. McGuinness, Y. Meng, A. Stacey, T. J. Karle, R. J. Hemley, N. B. Manson, L. C. L. Hollenberg, and S. Prawer, Phys. Rev. Lett. **112**, 047601 (2014).
[18] Y. Akahama and H. Kawamura, J. Appl. Phys. **96**, 3748 (2004).
[19] F. Occelli, P. Loubeyre, and R. LeToullec, Nat. Mater. **2**, 151 (2003).
[20] J.-P. Tetienne, L. Rondin, P. Spinicelli, M. Chipaux, T. Debuisschert, J.-F. Roch, and V. Jacques, New J. Phys. **14**, 103033 (2012).
[21] See Supplemental Material at http://link.aps.org/supplemental/10.1103/PhysRevB.107.L220102 for details about the experimental setup; details about the analytical model used; the fitting procedure used; extended data sets for measurements at additional pressure points and magnetic field orientation; partial information and data about ODMR contrast evolution with pressure; and analysis of magnetic sensitivity as a function of pressure, which includes Refs. [34–39].
[22] A. E. Hughes and W. A. Runciman, Proc. Phys. Soc. **90**, 827 (1967).
[23] A. Barfuss, M. Kasperczyk, J. Kölbl, and P. Maletinsky, Phys. Rev. B **99**, 174102 (2019).
[24] A. L. Ruoff, H. Luo, and Y. K. Vohra, J. Appl. Phys. **69**, 6413 (1991).
[25] M. L. Goldman, M. W. Doherty, A. Sipahigil, N. Y. Yao, S. D. Bennett, N. B. Manson, A. Kubanek, and M. D. Lukin, Phys. Rev. B **91**, 165201 (2015).

[26] J.-H. Dai, Y.-X. Shang, Y.-H. Yu, Y. Xu, H. Yu, F. Hong, X.-H. Yu, X.-Y. Pan, and G.-Q. Liu, Chin. Phys. Lett. **39**, 117601 (2022).

[27] S. Liu, Z. Li, Q. Jing, Y. Zhang, H. Ma, T. Tao, X. Wang, Y. Bi, J. Weng, and J.-a. Xu, Rev. Sci. Instrum. **85**, 046113 (2014).

[28] B. Li, C. Ji, W. Yang, J. Wang, K. Yang, R. Xu, W. Liu, Z. Cai, J. Chen, and H.-k. Mao, Proc. Natl. Acad. Sci. USA **115**, 1713 (2018).

[29] G. Shen, Y. Wang, A. Dewaele, C. Wu, D. E. Fratanduono, J. Eggert, S. Klotz, K. F. Dziubek, P. Loubeyre, O. V. Fatyanov, P. D. Asimow, T. Mashimo, R. M. M. Wentzcovitch, and other members of the IPPS task group, High Press. Res. **40**, 299 (2020).

[30] L. Rondin, J.-P. Tetienne, T. Hingant, J.-F. Roch, P. Maletinsky, and V. Jacques, Rep. Prog. Phys. **77**, 056503 (2014).

[31] S. Kolkowitz, A. Safira, A. High, R. Devlin, S. Choi, Q. Unterreithmeier, D. Patterson, A. Zibrov, V. Manucharyan, H. Park, and M. Lukin, Science **347**, 1129 (2015).

[32] R. D. Allert, K. D. Briegel, and D. B. Bucher, Chem. Commun. **58**, 8165 (2022).

[33] K. O. Ho, M. Y. Leung, W. Wang, J. Xie, K. Y. Yip, J. Wu, S. K. Goh, A. Denisenko, J. Wrachtrup, and S. Yang, Phys. Rev. Appl. **19**, 044091 (2023).

[34] R. Letoullec, J. P. Pinceaux, and P. Loubeyre, High Press. Res. **1**, 77 (1988).

[35] D. A. Broadway, B. C. Johnson, M. S. J. Barson, S. E. Lillie, N. Dontschuk, D. J. McCloskey, A. Tsai, T. Teraji, D. A. Simpson, A. Stacey, J. C. McCallum, J. E. Bradby, M. W. Doherty, L. C. L. Hollenberg, and J.-P. Tetienne, Nano Lett. **19**, 4543 (2019).

[36] F. Dolde, H. Fedder, M. W. Doherty, T. Nöbauer, F. Rempp, G. Balasubramanian, T. Wolf, F. Reinhard, L. C. L. Hollenberg, F. Jelezko, and J. Wrachtrup, Nat. Phys. **7**, 459 (2011).

[37] A. Dréau, M. Lesik, L. Rondin, P. Spinicelli, O. Arcizet, J.-F. Roch, and V. Jacques, Phys. Rev. B **84**, 195204 (2011).

[38] J. Kölbl, M. Kasperczyk, B. Bürgler, A. Barfuss, and P. Maletinsky, New J. Phys. **21**, 113039 (2019).

[39] J. F. Barry, J. M. Schloss, E. Bauch, M. J. Turner, C. A. Hart, L. M. Pham, and R. L. Walsworth, Rev. Mod. Phys. **92**, 015004 (2020).